Superelastic behavior and damping capacity of CuAlBe alloys

Susana Montecinos [a], María Ofelia Moroni [b,*], Aquiles Sepúlveda [c]

[a] *Universidad de Chile and CIMAT, Blanco Encalada 2008, Santiago, Chile*
[b] *Universidad de Chile, Depto. de Ingeniería Civil, Casilla 228/3, Santiago, Chile*
[c] *Universidad de Chile, Depto. de Ingeniería Mecánica, Casilla 2777, Santiago, Chile*

Abstract

Shape memory alloys (SMAs) showing the superelastic effect, dissipate energy through hysteretic cycles up to large strain amplitudes, without remnant strains after unloading. This effect is associated with a reversible stress-induced martensitic transformation. In this paper, the behavior of copper-based SMAs is examined, with the perspective of potential applications in seismic-energy dissipative devices. In particular, two different compositions of CuAlBe are characterized using chemical analysis, differential scanning calorimetry (DSC), light and scanning electron microscopy and X-rays diffraction. Mechanical and hysteretic damping properties are determined from cyclic tensile and tension–compression tests, for different strain amplitudes and frequencies. Both alloys show superelastic behavior, although hysteresis loops differ, due to differences in the composition and transformation phase temperatures. Equivalent damping up to 5% was obtained for the largest strain imposed. Frequency, in the range of interest for seismic applications, had a small influence on the damping values. It is concluded that alloy Cu–11.8 wt.% Al–0.5 wt.% Be best exhibited properties for the application intended.

Keywords: Shape memory alloys; CuAlBe alloy; Damping capacity

1. Introduction

A shape memory alloy (SMA) is a material which, in relation to the diffusionless martensitic phase transformation, may exhibit the shape memory effect or the superelastic effect (SE). The SE is associated with a large nonlinear recoverable strain upon loading and unloading, where an increasing stress applied to austenite gradually induces a considerable strain and the associated transformation into martensite. When the force is removed, the reverse martensitic transformation takes place, and the original material shape is recovered. Moreover, in both effects, energy dissipation (damping) is observed during load–unloading cycles.

In the stress-free state, a SMA is characterized by four transformation temperatures: M_s and M_f during cooling, and A_s and A_f during heating. M_s and M_f indicate the temperatures at which the transformation to martensite starts and finishes, respectively. A_s and A_f indicate the temperatures at which the inverse transformation starts and finishes, respectively. Moreover, above a temperature, usually called M_d, the stress induced martensitic transformation will not occur, because of the stability attained by austenite. Thus, for the SE to occur, stress should be applied within a temperature range between A_f and M_d, with $A_f < M_d$.

The damping behavior exhibited by superelastic materials makes them promising candidates to be used in seismic-energy dissipative devices. Although several shape memory alloys have been characterized, only few studies, using Cu-based SMA alloys, have been performed that are expected to lead to seismic applications [1,2]. In this case, it is desirable that the superelastic behavior occurs at ambient temperature. In addition, the material should dissipate substantial seismic energy through repeated stable cycles at large strains with little degradation in properties and low sensitivity to frequency in the 0.1–5 Hz range. Moreover, to avoid intergranular brittle fracture, a small grain size is needed.

Although the main factor controlling the temperature at which phase transformation takes place is alloy composition, others factors such as heat-treatment, quenching rate and grain size also affect this critical temperature [3]. For several compositions of the CuAlBe alloy, Table 1 shows the temperature phase transformation M_s reported by different authors, although neither the heat-treatment method nor the measurement procedure

* Corresponding author. Tel.: +562 9784372; fax: +562 6892833.
E-mail address: mmoroni@cec.uchile.cl (M.O. Moroni).

Table 1
Composition and M_s for CuAlBe alloy reported by different authors and calculated with Eqs. (1) and (2)

Alloy [ref.]	Al (wt.%)	Be (wt.%)	M_s (°C)	M_s (°C) Eq. (1)	M_s (°C) Eq. (2)	Notes
1 [5]	9.02	0.77	36	17.6	−83.03	10 min at 850 °C, quenching in 5% KOH 20 °C
2 [5]	9.55	0.86	−23	−32.37	−201.03	10 min at 850 °C, quenching in 5% KOH 20 °C
3 [5]	11.46	0.59	−32	−32.96	−95.53	10 min at 850 °C, quenching in 5% KOH 20 °C
4 [6]	11.9	0.5	−42	−24.7	−46.4	15 min at 650 °C, quenching in water at 100 °C
5 [11]	11.6	0.52	−10	−17.84	−42.98	No TT informed
6 [12]	11.4	0.6	−105	−33.4	−100.2	Drawing and quenching at 100 °C
7 [13]	11.65	0.47		−4.89	−1.86	–
8 [13]	11.5	0.49	−22.15	−4.48	−9.07	–
9 [13]	11.63	0.5	−33.15	−13.09	−27.23	–
10 [13]	11.79	0.59	−52.15	−47.15	−118.96	–
11 [13]	11.5	0.6	−120.15	−37.7	−107.3	–
12 [14]	11.36	0.78		−86.04	−258.1	Single crystal
13 [14]	11.65	0.47	−13.15	−4.89	−1.86	Single crystal
14 [15]	11.0	2.0	−14	−4.39	−1322	
15 [16]	11.5	0.5	−40	−7.5	−18	15 min at 650 °C, water quenching at 100 °C

are given for all of them. Empirical formulae such Eq. (1) [4] and Eq. (2) [5] have been proposed for two different heat-treatment and measurement procedures:

$$M_s = 1245 - 71(\text{wt.\% Al}) - 893(\text{wt.\% Be}) \quad (1)$$

$$M_s = 638 - 43(\text{wt.\% Al}) - 302(\text{wt.\% Be}) \quad (2)$$

Belkahla et al. [4] measured M_s by DSC in a polycrystal heated at 850 °C for 5 h, and water quenched; while Higuchi et al. [5] employed electrical resistivity in a material heated for 10 min at 850 °C, followed by quenching to 20 °C. Both equations show that the effect of the Al and Be content in the alloy is to decrease M_s, the effect of Be being much stronger than that of Al. As can be seen in Table 1, both equations coincide only partially with reported data. Neither of the equations includes the grain size, which is a variable that also affects the transformation phase temperatures.

Aging temperature and aging time are other factors that influence the behavior of the CuAlBe alloy and its phase transformation temperatures. Flores Zúñiga et al. [6] varied the aging time from 5 min to 500 h (at 250 °C) and the corresponding M_s changed from −42 to −15 °C.

This paper examines the suitability of superelastic CuAlBe SMAs for use in energy dissipation devices for civil engineering structures. In particular, results obtained from cyclic tests under tension and tension–compression loading of bars and wires are reported, as a function of strain amplitude and frequency. In addition, in order to characterize the alloys, several tests were performed: chemical analysis, differential scanning calorimetry, light and scanning electron microscopy, fractography and X-rays diffraction. The CuAlBe alloy came from two batches that were produced by Trefimetaux S.A., France.

2. Experimental procedure

Specimens from two different polycrystalline CuAlBe alloys, here called A and B alloys, having different diameters were employed.

Alloy A had a nominal composition of Cu–12.8 wt.% Al–0.6 wt.% Be and came as $\phi = 15$ mm bars, in the as-drawn and heat treated states, and also as heat-treated 1.4 mm wires. The thermal treatment consisted of 30 min at 700 °C and water quenching. The transformation temperature A_s was reported as −110 °C.

Alloy B had a nominal composition of Cu–11.8 wt.% Al–0.5 wt.% Be and came in the form of 3 mm wires and 5.6 mm diameter bars. According to the manufacturer, the phase transformation temperatures were $M_s = -18$ °C, $M_f = -47$ °C, $A_s = -20$ °C and $A_f = 2$ °C. These temperatures were also measured through DSC, giving $M_s = -5$ °C, $A_s = -9$ °C and $A_f = -4$ °C for 3 mm diameter wire and $A_s = -12.38$ °C for the 5.6 mm bar. These values are sufficiently close to constitute a verification of the manufacturer's specifications.

Optical microscopy was employed to identify the phases that were present and to measure the pertinent mean grain size, d, through lineal analysis. Also, X-rays diffraction was employed to identify the phases that were present.

A 50 kN MTS machine was used to perform static and dynamic tension–compression tests at room temperature. This machine may be configured to use feedback control of strain or stress to produce a sinusoidal load or deformation on the sample. The strain was measured with an extensometer that has a 25 mm gauge length, unless otherwise stated. Several tests were performed on both alloys by varying the type of control, the maximum stress or strain attained and the frequency. Hysteresis loops were obtained for each test, from which the secant stiffness, K, the energy loss per cycle, A_c, and equivalent damping ratio, β, were computed. K was calculated as the difference between the maximum and minimum stresses divided by the difference between the maximum and minimum strains, while β was calculated as (cycle area × 100) divided by (2π × area under the cycle loading curve) [7]. Fractographic analysis of the fractured tensile test specimens was performed using a scanning electron microscope, and the evolution of specimen temperature during some mechanical tests, due to adiabatic heating, was mea-

sured with *K* thermocouples fixed with elastic bands to the wire specimen.

Mechanical tests were performed on heat-treated specimens, coming from bars of alloy A ($\phi = 15$ mm) and alloy B ($\phi = 5.6$ mm). Specimens were machined with reduced gage diameters and heads. The gage diameters (ϕ_g) were 7 and 3.5 mm, respectively, while head diameters were equal to the original bar diameters. The distance between clamps was about 50 mm. In the case of wires of alloys A ($\phi = 1.4$ mm) and B ($\phi = 3$ mm), wire pieces were directly used as tensile specimens ($\phi_g = \phi$), leaving 100 and 50 mm between clamps, respectively.

Cyclic tension–compression tests using stress control were performed on alloy A specimens with $\phi_g = 7$ mm. Three maximum stresses were chosen, ±400, ±450 and ±500 MPa. For strain control tensile tests three maximum strains were chosen: 1, 1.5 and 1.8%. Up to 20 cycles were performed at each amplitude and frequency. Frequencies varied from 0.1 to 2 Hz, typical of the predominant frequencies of structures exposed to earthquakes. Additionally, slightly pre-strained wires ($\phi_g = 1.4$ mm) were tested in tension. In this case, four maximum strains were chosen: 1, 1.5, 2 and 2.5%. Up to 10 cycles were performed at each amplitude and frequency, where frequencies varied from 0.1 to 2 Hz [8].

For alloy B ($\phi_g = 3$ and 3.5 mm), two types of cyclic tensile tests were performed, at a frequency of 1 Hz and controlled by strain. The first one, labelled "increasing strain series type" consisted of successive cycle series performed at increasing strains. Each series included five load–unload cycles performed at the same maximum strain (or strain amplitude), e_m. One specimen was used in this test, and the strain amplitude values imposed were $e_m\% = 0.1$, 0.4, 0.7, 1.1, 1.4, 1.7, 2.0, 2.3, 2.6, 2.8, 3.0, 3.2 and 3.4%. The other type of cyclic tests, labelled "iso-strain series type" consisted of successive cycle series performed at the same level of maximum strain. Each series consisted of 10 load–unload cycles performed at the same maximum strain, with between 5 and 10 series applied successively. In the iso-strain series tests, one specimen was employed for each strain amplitude applied. These strain amplitudes, $e_m\%$, were: 0.9, 2.0 and 2.3%. Moreover, tensile tests were performed in a monotonic mode, without using an extensometer, at a crosshead speed of 1.6 mm/s at the laboratory temperature of 24 °C. The $\phi_g = 3$ mm and 3.5 mm specimens were austenized (betatized) for 2.5 and 4 min at 850 °C, respectively; followed by a conventional age hardening treatment applied for 1 h at 100 °C.

3. Results

3.1. Microstructure

Optical microscopy observations for both heat-treated alloys revealed a single-phase austenitic microstructure. The austenitic mean grain size, *d*, measured for each kind of specimens, is presented in Table 2. X-ray diffraction analysis confirmed, for both alloys, that only a cubic body-centred phase, austenite, was present.

Table 2
Initial diameter, gage diameter, and grain size of the materials considered

Alloy	As-received shape	Initial shape diameter, ϕ (mm)	Gage diameter, ϕ_g (mm)	Mean grain size, *d* (mm)
A	Wire	1.4	1.4	0.14
	Bar	15	7	0.45
B	Wire	3	3	0.4
	Bar	5.6	3.5	0.5

3.2. Composition and transformation temperature

Heat-treated alloy A ($\phi_g = 7$ mm) exhibited $A_s = -110$ °C and a grain size of 0.45 mm. Therefore, M_s is less than −110 °C. Using Eq. (2) for this A composition, a calculated value of $M_s = -93.6$ °C is obtained. After heat-treatment, the grain size of alloy B ($\phi_g = 3$ mm) attained $d = 0.4$ mm with $M_s = -5$ °C. Again using Eq. (2), a value of $M_s = -20.4$ °C was obtained for this composition. In this case, there is a reasonable agreement between both experimental results and the calculated values through Higuchi's equation. M_s is quite different between the two alloys because alloy A has a greater content of Be and Al and both elements decrease M_s. Incidentally, when Eq. (1) was applied to the same alloys, calculated M_s values were significantly smaller than experimental values. It is possible that, partially at least, this is due to the heat treatment applied by Belkahla, consisting of 5 h at 850 °C, which might have produced *d* values much larger than the present 0.4–0.5 mm. In fact, with a greater grain size, M_s is expected to be lower [9].

3.3. Hysteresis loops and damping capacity

All specimens have superelastic behavior at room temperature with stable cycles when subjected to dynamic tests, independent of the frequency and the type of control (strain or stress). Fig. 1 shows the stress–strain curve for a tension–compression test ($\phi_g = 7$ mm, alloy A) with stress controlled at a frequency of 1 Hz. In this case, the equivalent damping ratio, β, is 2.0%.

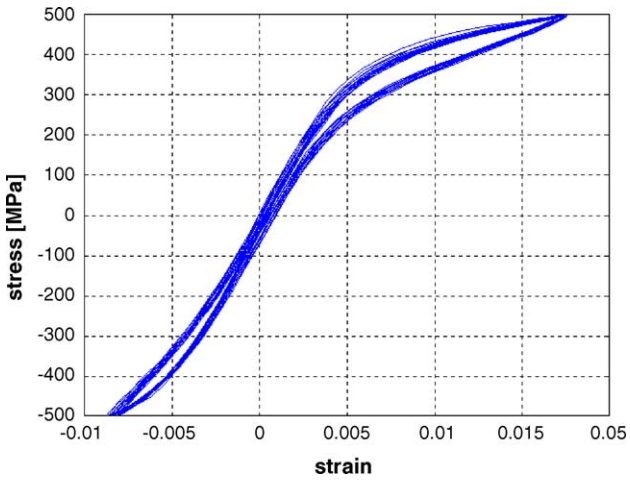

Fig. 1. Stress–strain curves of alloy A bar, $\phi_g = 7$ mm, under tension–compression cyclic loading, stress control test, frequency = 1 Hz.

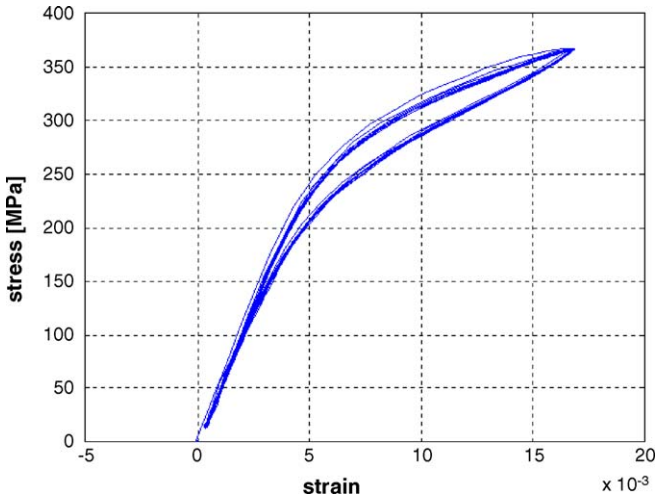

Fig. 2. Stress–strain curves of alloy A bar, $\phi_g = 7$ mm, under tension cyclic loading, strain control test, frequency = 1 Hz.

The curve is quite asymmetric with respect to zero strain. Fig. 2 shows the stress–strain curve for a tension test ($\phi_g = 7$ mm, alloy A) with strain controlled at a frequency of 1 Hz. The equivalent damping ratio is 1.12%. The maximum tensile strain attained in the tests performed on this type of bar was 1.97% and the maximum compression strain attained was 0.7%, both occurring at a maximum stress of ±500 MPa and at a frequency of 0.5 Hz.

Fig. 3 compares stress–strain curves for ϕ_g 7 mm specimens (alloy A) tested in tension at 0.5 and 1 Hz with the stress–strain curve from a stress controlled tensile test of the $\phi_g = 3$ mm wire (alloy B) performed at 0.5 Hz, for similar strain amplitudes. The minor influence of the test frequency is apparent. In addition, the energy loss per cycle (area of the hysteresis loop) for alloy B is much larger than the corresponding values for alloy A.

The forward transformation stress, corresponding to the stress at which the initial lineal stress–strain behaviour is lost, was established from Fig. 3 as 200 MPa for alloy A and 90 MPa for alloy B. Comparing alloys A and B, with similar grain sizes but different compositions, alloy A has a smaller M_s (<−110 °C) than alloy B (<−5 °C) and a higher transformation stress than alloy B. These results are in agreement with those of Guilemany and Gil [9], who show that M_s and the transformation stress are inversely proportional. When M_s is closer to (and below) the service temperature, the transformation of austenite into martensite is easier and, consequently, the corresponding transformation stress is smaller.

Table 3
Equivalent damping of CuAlBe wires

Diameter	Frequency (Hz)	Maximum stress (MPa)	Maximum strain (%)	Damping (%)
Alloy A ($\phi = 1.4$ mm)	0.1	396	0.98	0.57
	0.5	356	1.46	1.12
	0.5	411	1.94	1.27
	0.5	451	2.40	1.50
	1.0	477	1.93	1.13
	1.0	477	2.38	1.59
Alloy B ($\phi = 3$ mm)	0.1	170	0.8	4.08
	0.5	170	1.4	4.06
	0.5	200	2.0	4.61
	0.5	230	2.85	5.34
	1.0	200	2.0	4.91

Table 3 compares the equivalent damping ratios obtained from tensile cycle tests on ϕ_g 1.4 and 3 mm wires; values from alloy B are much larger than for alloy A, for the same strains.

3.4. Monotonic tensile tests and fractographic analysis

Results of a monotonic tensile test on ϕ_g 3 mm wire (alloy B) are shown in Fig. 4. The forward transformation stress occurred at 170 MPa. Fracture occurred at a stress of 515 MPa and for a total strain of 15.2%. Moreover, it was found that the average temperature increase due to adiabatic heating was about 2.3 °C/s, with a total temperature rise of 12 °C. In alloy B, fracture occurred at 500 MPa for a strain below 3% during dynamic tensile test.

Fig. 5 compares the fracture surfaces obtained from SEM fractographic analysis for both materials. While fracture of alloy A occurred due to a brittle intergranular mechanism, the fracture surfaces of alloy B were transgranular with a mixed cleavage-ductile mechanism. In effect, cleavage facetted regions were observed to coexist with adjacent dimpled ones, within a given grain.

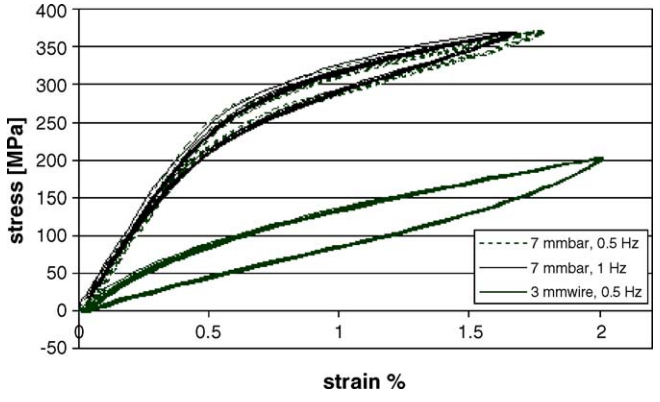

Fig. 3. Comparison of hysteresis loops $\phi_g = 7$ mm, alloy A and $\phi_g = 3$mm, alloy B specimens.

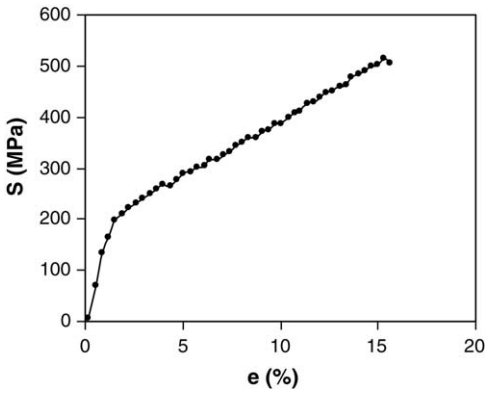

Fig. 4. Engineering tensile curve for ϕ_g 3 mm alloy B wire.

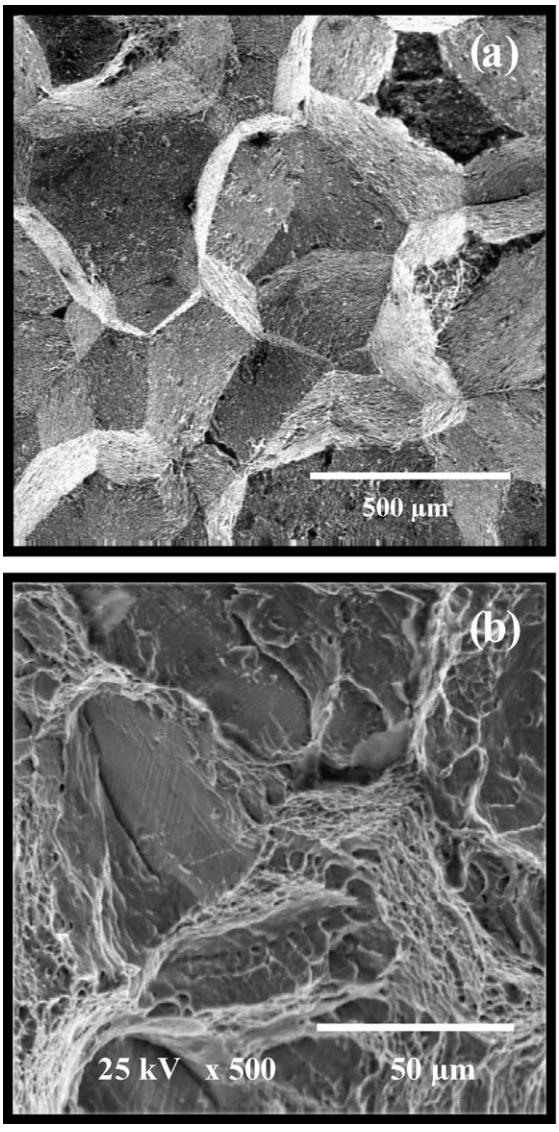

Fig. 5. Fractography of heat-treated tensile specimens: (a) Cu–12.8 wt.% Al–0.6 wt.% Be alloy and (b) Cu–11.8 wt.% Al–0.5 wt.% Be alloy.

Given the low A_c and β values, and the brittle type of failure exhibited by alloy A, as compared to what was observed for alloy B, it was decided to study only specimens coming from alloy B in more depth.

3.5. Superelastic range upper limit

One specimen from alloy B was submitted to cyclic tensile tests of the iso-strain series type. The corresponding cyclic stress–strains curves are shown in Fig. 6 for selected e_m values. In these curves, hysteresis loops which close near the origin are observed. Moreover, as e_m increases, the shape of the corresponding stress–strain loops changes. Note that in successive series, the strain rate increases for these tests.

In each specimen, the deformation imposed was fully recoverable up to a given e_m value, within experimental error limits. Such e_m values will be called hereafter as the superelastic upper limit in deformation (SEULD). The cycles of any series performed below or up to the SEULD, showed good reproducibility in the strain–stress plane, except for the first cycle of each series. So, the cycles represented in Fig. 6 correspond to the second cycle of each series.

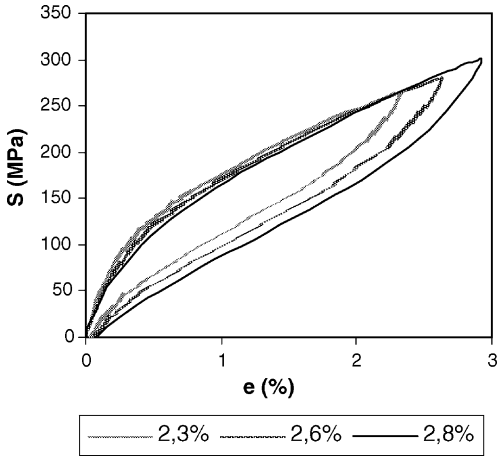

Fig. 6. Stress–strain curves for the cyclic tensile test of the increasing-strain series type, alloy B. For clarity, only the second cycle of some selected series is shown.

It was estimated that the measurement error for determining the remnant strain is $e_m\% = 0.05$. Thus, within experimental error, SEULD values of 2.3% are determined. This SEULD result is a lower limit; the upper limit corresponds to the next strain value of the succession of imposed e_m values.

Similar tests were also performed with 5.6 mm diameter rods of the same alloy, employing machined tensile specimens with a gage diameter of 3.5 mm. Good agreement was found between both specimen behaviours. A SEULD of 2.6% was determined for this bar dimension.

Tests of the iso-strain series ($e_m\% = 0.9$, 2.0, and 2.3%; 1 Hz) showed that, in a given test, after many series of cycles at the same amplitude, the stress–strain cycles remained stable and have no remnant strain, at least within an acceptable experimental error. It was also verified that as the strain amplitude of the tests was increased, the shape of the cycles changed. All of these observations are in close agreement with what was reported above regarding results of the increasing-strain tests. Some of these results will be presented quantitatively in Section 3.7.

3.6. Temperature evolution during cyclic tensile tests

Evolution of the temperature during the cyclic tensile test of increasing strain on a ϕ_g 3 mm specimen is shown in Fig. 7. Some corresponding stress–strain cyclic curves were already shown in Fig. 6. The time between cycles was chosen to be sufficiently long so that every cycle started at room temperature (24 °C). Unfortunately, the rate at which the temperature data was recorded was too low (only 1 Hz, compared to that of the mechanical cycling frequency, also of 1 Hz), to obtain an adequate resolution. Thus, each temperature peak observed in Fig. 7 corresponds to a few random data in one series. Nevertheless, the plot shows that as the strain amplitude increased from series to series, the maximum temperature attained also increased. Moreover, it is noted that for $e_m = 2.3\%$, a tempera-

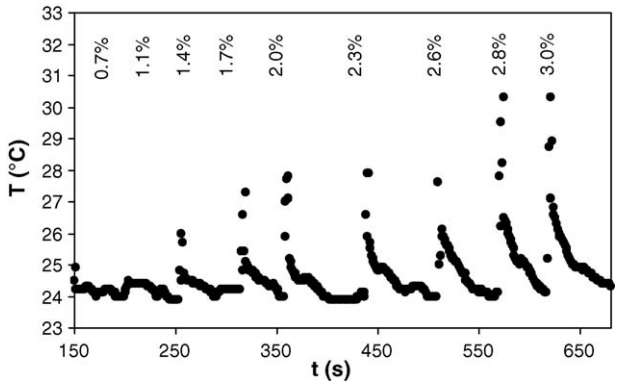

Fig. 7. Evolution of temperature vs. time during an increasing-strain series type test with alloy B. The strain amplitude of each series is indicated in the figure.

ture increase of about 4 °C was detected after the pertinent series of five cycles.

The thermal results of cycling tests of the iso-strain series type showed a general good agreement with those presented above for the increasing-strain series type.

Concerning the adiabatic heating results presented in Fig. 7, the increase of temperature with larger strain amplitude was explained by Torra et al. [10]: cycling produces heat dissipation due to frictional effects and latent heat. Temperature increase in the alloy depends on the cycling frequency, the thermal coupling with the surroundings, the cross section of the samples and the deformation percent. Under the present experimental conditions, larger strain amplitude means faster cycles for a given frequency, and a larger volume fraction of transformed martensite. These two factors should increase the heat produced, in each cycle, due to frictional effects.

3.7. Strain effects

It has already been shown that strain–stress loops corresponding to the increasing-strain series type of cyclic tensile tests change their shape with increasing strain, see Fig. 6. The following significant features, from the perspective of civil engineering design, were determined and their evolution with strain represented:

- Secant stiffness, K, see Fig. 8a: K decreases sharply for small strains and converges to an almost constant value for larger strains.
- Energy dissipated in each cycle, A_c, corresponding to the area of the loop, Fig. 8b: A_c increases more than linearly with strain.
- Equivalent damping ratio, β, see Fig. 8c: β increases almost linearly for strains larger than 0.6%.

Fig. 8 also contains, with full circles, the results corresponding to the three iso-strain series type tests. Both types of test results agree in terms of K and A_c values. Regarding damping ratio, there are some differences. A similar tendency was obtained from tests on alloy A, although for that material damping values were too small for the application pursued in this project.

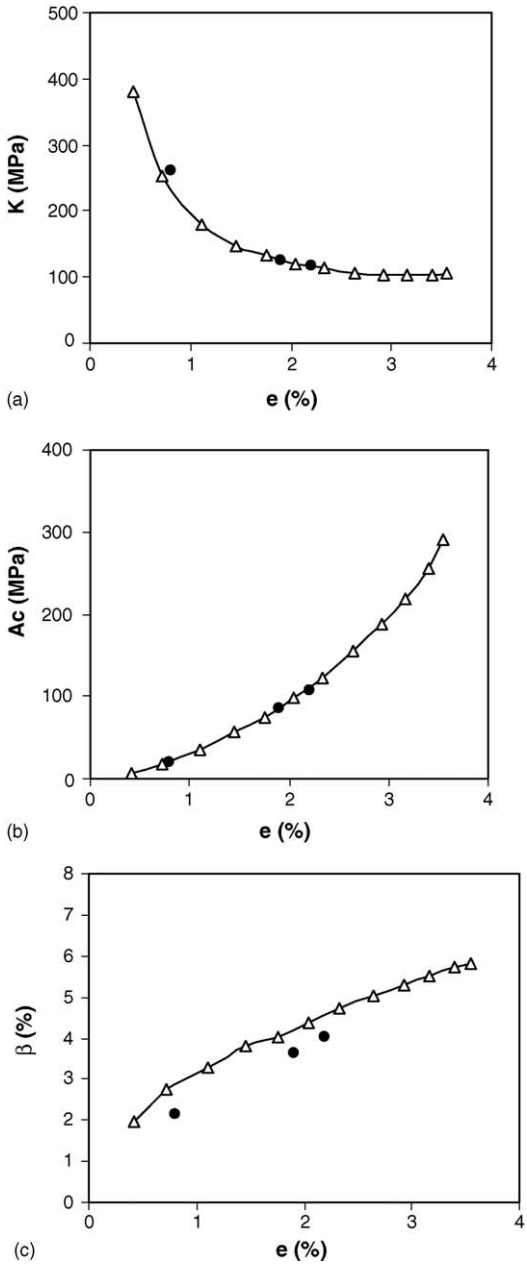

Fig. 8. Evolution of different parameters of the stress–strain loop curves with amplitude strain, in increasing-strain series type tests performed at 1 Hz: (a) secant stiffness, K (MPa) (b) energy dissipated per cycle, A_c and (c) equivalent damping ratio, β%.

4. Conclusion

Two commercial batches of CuAlBe alloy have been characterized. Nominal composition differed in 1% Al and 0.1% Be. Both alloys present an austenitic microstructure and the superelastic effect. Nevertheless, important differences between the alloys were evident in terms of transformation phase temperatures, phase transformation stresses, hysteresis loop shapes, damping capacity and type of fracture. These differences in properties can be mainly ascribed to the difference in compositions between the present alloys; thus, the effect of alloy composition on phase transformation temperatures and, conse-

quently, on phase transformation stresses, was discussed. Alloy B (Cu–11.8 wt.% Al–0.5 wt.% Be) showed a promising behavior for use in seismic dissipation devices: the superelastic effect was observed for strains up to 2.3% and equivalent damping reached a 4% for the said strain; also, in static tensile tests, the fracture strain was approximately 15%, with a transgranular fracture mechanism. Additional studies, however, need to be performed before full-scale application is warranted.

Acknowledgments

The authors acknowledge research grant FONDECYT No. 1030554, Chile, S. Montecinos is grateful to CIMAT, Chile, for financial support. The Ministerio de Obras Públicas, Chile, provided access to its MTS facility; the collaboration of Eng. Gabriel Palma is greatly appreciated.

References

[1] M. Dolce, D. Cardone, R. Marnetto, Earthquake Eng. Struct. Dyn. 29 (2000) 945–968.
[2] R. DesRoches, J. McCormick, M. Delemont, J. Earthquake Eng. 8 (2004) 415–429.
[3] T. Tadaki, in: K. Otsuka, C.M. Wayman (Eds.), Shape Memory Materials, Cambridge University Press, Cambridge, UK, 1998, pp. 97–116.
[4] S. Belkahla, H. Flores Zúñiga, G. Guenin, Mater. Sci. Eng. A169 (1993) 119–124.
[5] A. Higushi, K. Suzuki, Y. Matsumoto, S. Komatsu, Y. Nakamura, J. Phys. IV France 12 (C4) (1992) 767–771.
[6] H. Flores Zúñiga, D. Ríos Jara, S. Belkhala, V. Nika, G. Guénin, Scr. Mater. 12 (1996) 1899–1904.
[7] Y. Liu, J. Van Humbeck, J. Phys. IV France 7 (C5) (1997) 519–524.
[8] C. Adasme, Mech. Eng. thesis, University of Chile, 2001 (in Spanish).
[9] J.M. Guilemany, F.J. Gil, Rev. Metal. Madrid 27 (5) (1991) 296–300.
[10] V. Torra, A. Isalgue, F.C. Lovey, F. Martorell, M. Sade, SMA and Dampers in Civil Eng.: Long Time Guaranted Behavior and Diffusional Phenomena, Actas de Jornadas SAM/CONAMET/ Simposio Materia 2003, Bariloche, Argentina (2003), paper 0526.
[11] A. Hautcoeur, A. Eberhardt, E. Patoor, M. Berveiller, J. Phys. IV France 5 (C2) (1995) 459–464.
[12] Y. Gillet, E. Patoor, M. Berveiller, Beam Theory Applied to Shape Memory Alloys. Proceedings of the First International Conference on SMA and Superelastic Technologies, Pacific Grove, CA, USA, 1994, pp. 169–174.
[13] D. Ríos-Jara, A. Planes, Ll. Mañosa, J. Ortin, S. Belkahla, M. Morin, G. Guénin, J. Macqueron, J. Phys. IV France 1 (C4) (1991) 283–288.
[14] D. Ríos-Jara, S. Belkahla, A. Canales, H. Flores, G. Guénin, Scr. Metall. Mater. 25 (1991) 1351–1355.
[15] C. Bouvet, S. Calloch, C. Lexcellent, D. Marquis. Mechanical Behavior of CuAlBe Shape Memory Alloy under Multiaxial Compression Loadings, ICM8 vol. III.5 Smart Materials, 1999, pp. 939–943.
[16] H. Flores Zúñiga, D. Ríos Jara, F. Lovey, G. Guénin, J. Phys. IV France 5 (C2) (1995) 171–174.